

Analytical modeling of the evaporation of sessile drop linear arraysS. Tonini^{*} and G. E. Cossali*Department of Engineering and Applied Sciences, University of Bergamo Viale Marconi 5, 24044 Dalmine, Bergamo, Italy*

(Received 11 February 2022; accepted 28 April 2022; published 16 May 2022)

An analytical model for predicting the competitive evaporation of two and three sessile drops is proposed, based on an analytical solution, in terms of Mehler functions, of the steady species and energy conservation equations for the gaseous phase. The assessment through a comparison with accurate numerical solutions of the species conservation equations is reported in order to quantify the accuracy of the analytical solution. The model is validated against three available sets of experiments on two and three sessile drops on a line array. The decrease of the evaporation rate caused by the vicinity of sessile drops is reported in terms of a screening coefficient given by a relatively simple analytical expression. The influence of wall wettability on the evaporation of pairs of sessile drops is analyzed, and a parameter is proposed to quantify the effect of geometry in a unified way.

DOI: [10.1103/PhysRevE.105.054803](https://doi.org/10.1103/PhysRevE.105.054803)**I. INTRODUCTION**

Evaporation of liquid drops deposited on substrates is a phenomenon playing a crucial role in many scientific, biological, and industrial applications, such as ink-jet printing [1], pesticide spraying [2], micro- and nanofabrication [3], film coatings [4], spray cooling [5], deposition of DNA/RNA micro-arrays on solid surfaces [6], and many others.

This has motivated extensive analytical, experimental, and numerical investigations on sessile drop evaporation (refer to [7–9] for recent reviews on this topic) addressing the complexity of the many phenomena occurring, such as thermal Marangoni effects [10], contact line instabilities [11], drop shape [12], effect of substrate conductivity [13], effect of particle suspensions [14], etc.

Two limiting modes of drop evaporation were evidenced (see, for example, [12,15]), which depend upon the motion of the triple-phase contact line: the constant-contact-radius (CCR) mode, where the drop contact line is pinned and the contact angle decreases during evaporation, and the constant-contact-angle (CCA) mode, characterized by the motion of the contact line while the contact angle remains constant. Transitions between these limits are generally observed, and a third mode, called stick-slip mode [16], characterized by simultaneous variations of the contact angle and the contact line, is observed. Experiments of water droplets deposited on metal and polymer substrates shows that the evaporation follows a different behavior on weakly pinning (polymer) and strongly pinning (metallic) surfaces [17]. When deposited on polymer surfaces, the droplet evaporates according to a stick-slip sliding motion, characterized by the oscillation of the contact angle around some value as the drop radius decreases, steadily or with jumps, while on strong-pinning metallic surfaces an extremely large contact-angle hysteresis is observed.

Moreover, the substrate characteristics, in particular the wettability, are shown to be responsible for the mode of evaporation and the overall lifetime of the vaporizing drops [18].

When a drop vaporizes in a gaseous environment the diffusion of vapor from the droplet is the main physical mechanism controlling the evaporation, then a “diffusion-limited model” is used to describe the process [19]. When the timescale of evaporation is orders of magnitude higher than the diffusion timescale, the quasisteady assumption may become acceptable and the problem of the species transport from a liquid spherical cap into the gaseous phase reduces to the solution of the Laplace equation, which has an explicit analytical form in toroidal coordinates [20] that has been widely used in analytical modeling.

The focus of the research on sessile drop evaporation has been expanded to the study of multiple droplets, due to the many applications where this phenomenon is encountered [8,21]. The presence of neighboring droplets on the same substrate increases the local vapor concentration then decreasing the evaporation rate of each individual droplet, depending on the closeness of the surrounding droplets. This is often referred to as a “shielding” effect, which has been shown to influence the drop lifetime, the flow structure, and in some cases the morphology of the final deposits, and it can lead to asymmetric deformation of the drops [22] and alteration of evaporation modes [23]. The shielding effect reduces as the separation distance between droplets increases, and beyond a certain threshold value, which depends also on the properties of the hydrophobic substrate [24], it may become negligible. The effect of interdrop spacing on the dynamics of drop evaporation and condensation has been experimentally investigated by many authors. An increment of the number of drops in ordered drop arrays was shown to increase the lifetime of the central and outer droplets [21], and the decrease of drop spacing in large drop arrays causes a modification of the evaporation behavior. When drops become very close, the evaporation mode approaches that of a continuous film,

*Corresponding author: simona.tonini@unibg.it

with uniform vapor flux and drop volume reducing linearly with time, in contrast with the behavior of isolated drops, where the drop volume changes with time as $V \propto t^{3/2}$ [25]. Experiments on evaporation of isolated and interacting water drops on a polystyrene surface, with contact angle equal to 94° , showed the inception of an instability, already observed by [26], caused by the collective evaporation, which leads to nonuniform evaporation starting at the array boundary [27].

The analytical modeling of drop array evaporation has been approached in different ways. For example, time-dependent cooperative drop evaporation has been analyzed for quasi-one-dimensional [28] and two-dimensional [26] drop arrays through the solution to the Cahn-Hilliard equation. Quasisteady evaporation of groups of sessile drops is commonly modeled as a diffusion-limited phenomenon, reducing the complexity of the problem to the solution of the Laplace equation. Since the same mathematical problem appears in different fields of physics, methods used to model different phenomena and applications, like the diffusion mechanism from biological membranes [29], electrical conductance through multiple discrete contact interfaces [30], and diffusion of gas from pairs of nanobubbles on a flat surface [31], can be transferred to the modeling of sessile drop array evaporation. As an example, an asymptotic analytical model of evaporation for multiple sessile drops was recently proposed by [32], based on the integral approach of [29]. The model was derived for thin drops with circular basis, but it was shown by [33] that it can be extended to spherical caps in the hydrophilic range, a comparison with experimental interferometric measurements of structured and random 2D sessile drop arrays on hydrophilic surfaces (contact angle equal to $64^\circ \pm 4^\circ$) showed a rather satisfactory agreement.

The present work proposes a simple analytical model for the diffusion-limited vaporization from pairs and triplets of interacting liquid spherical caps on a solid substrate, by superposing existing solutions for single drops [20]. The model accounts for the presence of the Stefan flow and for the effect of temperature dependent thermophysical properties, by extending an existing analytical approach [34] to model the case of sessile drops. The next section describes the mathematical derivation of the model, followed by its numerical assessment, the comparison with experimental data from the literature and a collection of results to quantify the shielding effect for different drop pair configurations on hydrophobic and hydrophilic substrates.

II. MATHEMATICAL MODEL

The shape of a sessile drop is governed by gravity and surface wettability, which is defined by the contact angle, $\theta_c = \pi - \psi_0$, (see Fig. 1). In the following, the size of the drop will be assumed to be small when compared to the capillary length $(\sigma/g\rho_L)^{1/2}$, where σ is the surface tension, g is the gravitational acceleration, and ρ_L is the liquid density, so that the drop shape can be approximated by a spherical cap.

Moreover, the terms hydrophilic and hydrophobic will be used to describe drop-substrate configurations where $\theta_c < \pi/2$ and $\theta_c > \pi/2$, respectively.

The sessile drops will be taken as single component and the gaseous phase is assumed to be an ideal binary mixture

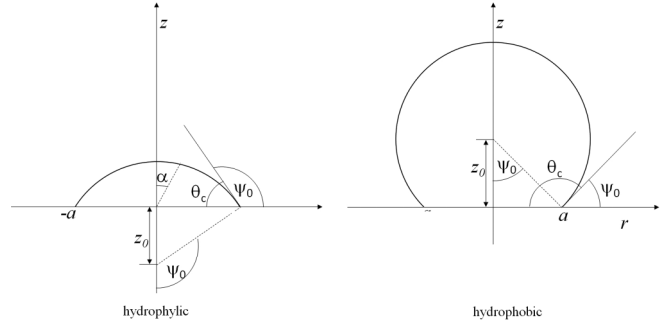


FIG. 1. Schematic of a sessile drop: (left) hydrophilic substrate and (right) hydrophobic substrate.

made by the evaporating species (vapor) and the ambient gas. Quasisteadiness will be assumed, and the heat and mass transfers in the gas mixture can then be modeled by solving the steady-state species and energy conservation equations:

$$\nabla_j N_j^{(p)} = 0 \quad (p = 0, 1), \quad (1)$$

$$\rho v_j \nabla_j (c_p^{(1)} T) = \nabla_j (k \nabla_j T), \quad (2)$$

where T is the gas temperature, $N_j^{(p)}$ are the molar fluxes defined as

$$N_j^{(p)} = N_j^{(T)} y_j^{(p)} - c D_{10} \nabla_j y_j^{(p)}, \quad (3)$$

where $y^{(p)}$ is the molar fraction of species p ($p = 0$ for the ambient gas and $p = 1$ for the evaporating component), c is the molar gas density, D_{10} is the binary mass diffusion coefficient, and $N^{(T)} = N^{(0)} + N^{(1)}$. The steady-state energy equation (2) takes into account interdiffusional terms, but it neglects dissipation by viscous stresses and further minor terms (refer to [35], p. 465, or [36], p. 589, for more complete forms for this equation), v_j is the mass average mixture velocity, ρ is the mass density, k is the gaseous mixture conductivity, and $c_p^{(1)}$ is the vapor-specific heat capacity. Mass fluxes, $n_j^{(p)}$, can be recovered from the molar fluxes by $n_j^{(p)} = M m^{(p)} N_j^{(p)}$, where $M m^{(p)}$ is the molar mass of species p . External convection is neglected with the exception of the fluid motion caused by the Stefan flow, which is then the only cause of the gas velocity v_j .

Uniform Dirichlet boundary conditions on the drop surface are considered for both temperature and molar fractions, and the wall is assumed adiabatic. Under these conditions an analytical solution of the problem set by Eqs. (1) and (2) can be obtained also when the thermophysical properties are assumed to depend on temperature [37] (with some simplifying assumptions on the kind of dependence; see also [34]). The quasisteadiness assumption implies that the drop surface can be considered still, and since the absorption of the ambient gas into the liquid can safely be taken as negligible, the flux $N^{(0)}$ is nil on the surface and, in the absence of external convection, it is nil everywhere. Introducing the nondimensional quantity $H = \ln(1 - y^{(1)})$, the species conservation equations, when thermophysical properties are independent of temperature, yield the following Laplace equation:

$$\nabla^2 H = 0. \quad (4)$$

In [34] it was shown that the problem set by Eqs. (1) and (2) can still be analytically solved also for thermophysical properties depending on temperature by power laws, by introducing a harmonic auxiliary function Φ , which satisfies the Laplace equation, and it is nil at infinity and equal to 1 on the drop surface, whatever the shape of the liquid-gas interface. In that case the fields H and T are given, in implicit form, in terms of Φ , but the heat flux, q_j , and the vapor flux, $n_j^{(1)}$, can be obtained (see also [37]) through the following relations:

$$n_j^{(1)} = f_n^{(1)} \nabla_j \Phi, \quad (5)$$

$$q_j = f_q \nabla_j \Phi, \quad (6)$$

where $f_n^{(1)}$ and f_q are constants defined by the thermophysical properties, while the gradient $\nabla_j \Phi$ depends only on the geometry of the problem. To notice that when the thermophysical properties are assumed constant, the auxiliary function becomes $\Phi = \frac{H-H_\infty}{H_s-H_\infty}$, where $H_s = \ln(1-y_s^{(1)})$ and $H_\infty = \ln(1-y_\infty^{(1)})$ are the boundary values on the drop surface and at infinity, respectively, and

$$f_n^{(1)} = Mm^{(1)}cD_{10}(H_s - H_\infty), \quad (7)$$

$$f_q = c_p^{(1)}(T_s - T_\infty) \frac{e^Y}{1 - e^Y} f_n^{(1)}, \quad (8)$$

where $Y = \frac{H_s - H_\infty}{Le_M}$ and $Le_M = \frac{k}{Mm^{(1)}cD_{10}c_p^{(1)}}$ is the modified Lewis number; see [34]. The evaporation rate, m_{ev} , and the sensible heat rate, Q , exchanged with the surrounding gas can then be found by integrating the normal component of the fluxes over the drop surface S :

$$m_{ev} = f_n^{(1)} \int_S \nabla_n \Phi dS, \quad (9)$$

$$Q = f_q \int_S \nabla_n \Phi dS. \quad (10)$$

The analytical solution to the Laplace equation in the outer field of a single sessile drop (for the geometry reported in Fig. 1) was first proposed by [20] making use of the toroidal coordinate system (ξ, ψ, φ) :

$$x = a \frac{\sinh(\xi)}{\Theta} \cos \varphi, \quad (11a)$$

$$y = a \frac{\sinh(\xi)}{\Theta} \sin \varphi, \quad (11b)$$

$$z = a \frac{\sin(\psi)}{\Theta}, \quad (11c)$$

$$\Theta = \cosh(\xi) - \cos \psi, \quad (11d)$$

where (x, y, z) are the Cartesian coordinates and a is the size parameter, which is equal to the drop base radius R_c (see Fig. 1). In this system the spherical cap shape can be represented by the simple equation $\psi = \psi_0$ and the function Φ as

$$\Phi = \sqrt{2}\Theta^{1/2} \int_0^\infty P_{i\tau-1/2}(\cosh \xi) \times \frac{\cosh[(\tau - \psi_0)\tau] \cosh(\psi\tau)}{\cosh(\tau\tau) \cosh(\psi_0\tau)} d\tau, \quad (12)$$

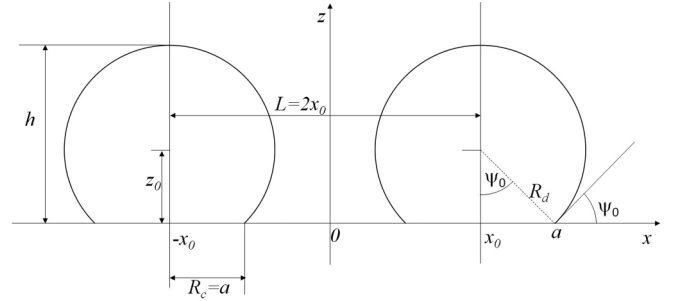


FIG. 2. Schematic of a pair of sessile drops: geometric parameters.

where $P_{i\tau-1/2}(x)$ are the Legendre functions of first kind with complex index, which are sometimes called conical or Mehler functions [38]. Equation (12) and some simplified forms were widely used to model the evaporation of sessile drops (see, for example, [39,40]), under the assumption of constant thermophysical properties and nil Stefan flow.

A. Model for two interacting drops

Let now consider a pair of identical sessile drops, which centers are separated by a distance L (refer to Fig. 2 for the geometric description).

An explicit analytic form of the auxiliary function Φ for this kind of geometry, satisfying uniform Dirichlet conditions on drop surfaces, is not known. However, a possible solution to the Laplace equation can be found by superposing existing solutions of single drops. Let $\Phi(x, y, z)$ be the solution for the case of a single sessile drop positioned at the origin, as shown in Fig. 1, i.e., such that its value on the surface $\psi = \psi_0$ (in toroidal coordinates) is equal to 1 and it is nil at infinity. Then $\Phi_1 = \Phi(x + x_0, y, z)$ and $\Phi_2 = \Phi(x - x_0, y, z)$ are the solutions for the case of a drop shifted left and right by a distance x_0 along the x axis, respectively (as in Fig. 2). The linear combination

$$\Phi_{12} = \gamma(\Phi_1 + \Phi_2) \quad (13)$$

is still a solution to the Laplace equation and it is nil at infinity, but it cannot satisfy the condition $\Phi = 1$ over the whole surface of the two drops. However, it is possible to choose γ such that the condition is satisfied at least on some points of the drop surfaces. A similar method is used, for example, to model the evaporation of free drop arrays and clouds by means of the point source approach (see, for example, [41]). To find a value for γ , it can be assumed that the boundary condition $\Phi = 1$ is satisfied on both drop apexes, and this can be better written in a shifted coordinate system, such that one of the drops is positioned at the origin and the other one is shifted by $2x_0$ along the x axis, i.e.,

$$1 = \gamma[\Phi(0, 0, R_d + z_0) + \Phi(2x_0, 0, R_d + z_0)], \quad (14)$$

where R_d is the drop curvature radius (see Fig. 2) and z_0 is the coordinate of the drop apex. Observing that $\Phi(0, 0, R_d + z_0) = 1$, the coefficient γ can be found as

$$\gamma = \frac{1}{1 + \Phi(2x_0, 0, R_d + z_0)}. \quad (15)$$

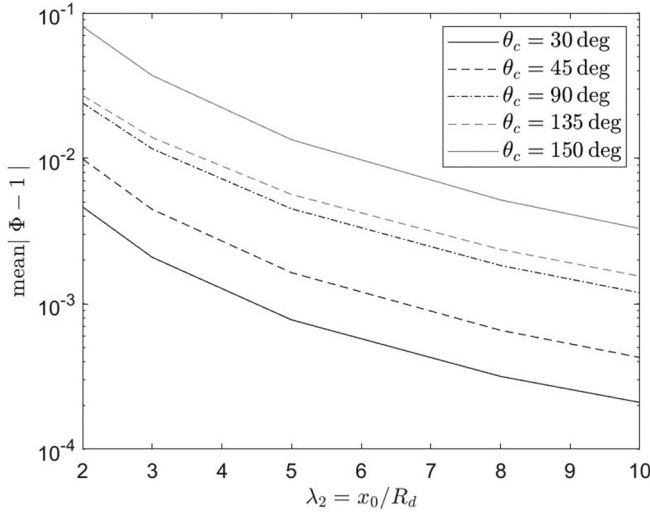


FIG. 3. Average values of the difference between the values of Φ_{12} on one of the drop surfaces and the correct boundary condition, as a function of drop interdistance $\lambda_2 = \frac{x_0}{R_d}$, for different contact angles.

It is now possible to check the discrepancy between the actual value of Φ_{12} over the surface of one of the two drops and the exact boundary condition $\Phi_{12} = 1$. The results are reported in Fig. 3, in terms of the average difference between the actual value of Φ_{12} on the surface and the exact boundary condition, for five values of the contact angle varying between 30° and 150° , as a function of the drop interdistance $\lambda_2 = \frac{x_0}{R_d}$.

To notice that this range of contact angles covers different surface wettability conditions. It is worth notice that the characterization of PTFE (Teflon) surfaces has shown that typical contact angles (for water drops) between 116° [42] and 122° [43] can be reached with an untreated surface having roughness of the order of 150 nm [42]. However, there exist treatments that can increase PTFE wettability over 150° [44] using ion beam irradiation maintaining the roughness below about 400 nm, and up to 165° [45] by surface extension (up to 190%) due to fibrous crystals' structure modification.

It is worth notice that the solution (12) for the case of a single sessile drop can be written in terms of simple analytic functions making use of the method of images, when $\psi_0 = \frac{\pi}{2N}$ and N is a positive integer (see also [46] and [47]), and then for these cases the calculation of Φ_{12} [Eq. (13)] is easy (see also [37]). For the other values of ψ_0 the numerical evaluation of Φ from Eq. (12) can be obtained by numerical integration, although computationally more expensive (see also [46] for a different approach).

For a comparison with available data, which are reported in the next section, the proposed method can be extended to the case of three drops on a line (see Fig. 4).

Considering again the solution for the single drop case $\Phi(x, y, z; \psi_0)$, let us take the superposition of the three fields corresponding to three drops separated by a distance $2x_0$:

$$\begin{aligned} \Phi_{12} = & [\gamma_s \Phi(x - 2x_0, y, z) + \gamma_c \Phi(x, y, z) \\ & + \gamma_s \Phi(x + 2x_0, y, z)], \end{aligned} \quad (16)$$

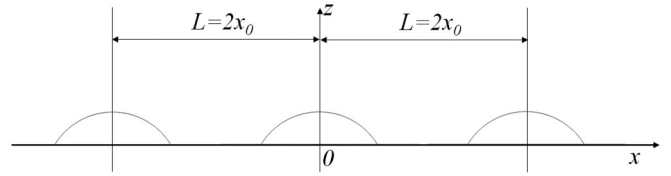


FIG. 4. Schematic of a triplet of sessile drops: three drops on a line configuration.

where the symmetry of the problem is used to diminish the number of coefficients. As above, the boundary condition cannot be uniform over the drop surfaces, and again let us impose the value $\Phi_{12} = 1$ on the drop apices. Using the symmetry of Φ , the condition at the apex of the central drop yields

$$1 = \gamma_c + 2\gamma_s \Phi(2x_0, 0, R_d + z_0), \quad (17)$$

while that on the outer drops can be written, by shifting one of the outer drop at the origin, as

$$1 = \gamma_s + \gamma_c \Phi(2x_0, 0, R_d + z_0) + \gamma_s \Phi(x + 4x_0, 0, R_d + z_0). \quad (18)$$

Defining for simplicity

$$\Phi_{2x_0} = \Phi(2x_0, 0, R_d + z_0), \quad (19a)$$

$$\Phi_{4x_0} = \Phi(4x_0, 0, R_d + z_0), \quad (19b)$$

the solution of the system (17) and (18) yields

$$\gamma_s = \frac{1 - \Phi_{2x_0}}{(1 + \Phi_{4x_0}) - 2(\Phi_{2x_0})^2}, \quad (20)$$

$$\gamma_c = \frac{1 + \Phi_{4x_0} - 2\Phi_{2x_0}}{(1 + \Phi_{4x_0}) - 2\Phi_{2x_0}\Phi_{2x_0}}. \quad (21)$$

The coefficients γ_s and γ_c can be directly related to the so-called screening factors, as discussed in the next subsection.

It is important to notice that once Φ_{12} is found, the method proposed in [34] can be used to find the distribution of vapor concentration and temperature taking into account the Stefan flow and the dependence of gas thermophysical properties on temperature. Since this method has been described in [34], it will not be discussed further here.

B. Evaporation rates

For the following analysis we can assume that the solution on the half space $z \geq 0$ can be extended to $z < 0$ by simply observing that $\Phi(x, y, z) = \Phi(x, y, -z)$, and consequently the drop shape can be intended as the actual drop plus its reflection on the lower half-space (see Fig. 5).

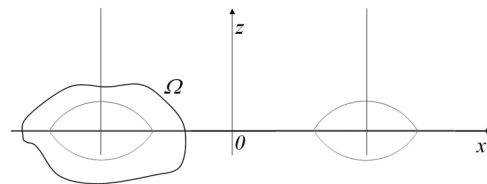


FIG. 5. Inner boundaries of the domain for the solution of the Laplace equation over all the space; Ω is a generic closed surface surrounding one of the inner boundaries.

Consider now any closed surface surrounding one single drop (surface Ω in Fig. 5). Since Φ is harmonic, the integral of the normal component of the gradient, $\nabla_n \Phi$, over this surface is independent of the choice of the surface, as far as it contains only one drop, and it is equal to the same integral taken over the drop surface. If the closed surface does not contain any drop, its value is nil. Referring to Fig. 5, let us then calculate the integral of $\nabla_n \Phi_{12}$ over the surface Ω :

$$\int_{\Omega} \nabla_n \Phi_{12} dS = \gamma \left[\int_{\Omega} \nabla_n \Phi_1 dS + \int_{\Omega} \nabla_n \Phi_2 dS \right], \quad (22)$$

where Eq. (13) is used. Since the closed surface does not contain the drop on the right, the integral $\int_{\Omega} \nabla_n \Phi_2 dS$ is nil, while $\int_{\Omega} \nabla_n \Phi_1 dS$ is that relative to the single sessile drop. Then, observing that the evaporation rate is proportional to those integrals [see Eq. (9)], the ratio

$$\gamma = \frac{\int_{\Omega} \nabla_n \Phi_{12} dS}{\int_{\Omega} \nabla_n \Phi_1 dS} \quad (23)$$

is equal to the ratio $\frac{m_{ev,1}}{m_{ev,is}}$ between the evaporation rate of one of the sessile drops, $m_{ev,1}$, and the evaporation rate of the same drop evaporating alone, $m_{ev,is}$. This quantity can be defined (as is done for free drops) as the *screening coefficient*, which accounts for the screening to the evaporation of one drop caused by the presence of the other one.

A similar argument can be used to show that, for the case of three drops on a line, γ_c and γ_s are the screening coefficients for the central and the side drops, respectively.

III. NUMERICAL ASSESSMENT

To evaluate the accuracy of the proposed analytical model for the evaporation of a pair of interacting sessile drops, the auxiliary function Φ was calculated through a 3D numerical approach using COMSOL Multiphysics® and compared with the analytical predictions for some conditions. The numerical solution of the Laplace equation is found using a finite element discretization approach, imposing uniform Dirichlet conditions on the boundaries corresponding to the drop-gas interface and to free stream conditions. Various configurations of single and a couple of interacting drops have been tested, varying the separation parameter $\lambda_2 = \frac{\lambda_0}{R_d}$ (refer to Fig. 1) from 2 to 10. The cases of a suspended drop (i.e., free spherical drops, formally identical to the case of a drop with contact angle equal to $\pi/2$) and of single sessile drops, with contact angle equal to 135° and 45° , have been considered, to represent hydrophobic and hydrophilic conditions. Taking advantage of the double symmetry of the problem, only one-eighth of the domain is simulated.

The main problem is encountered when setting boundary conditions at infinity, which must be substituted with boundary conditions at a finite distance from the drops, and this clearly affects the solution. The method used here to mitigate this problem is based on an iterative procedure, which can be described as follows. The boundary condition at infinity, which in this case is a nil value of the function Φ , is substituted with a finite uniform value of $\Phi_\infty^{(0)}$ on an outer spherical surface of radius R_∞ . After the first calculation, the values of the gradient $\nabla_n \Phi$, normal to the outer surface, are calculated and

used to evaluate a new boundary condition $\Phi_\infty^{(1)} = \Phi^{(1)}(R = R_\infty)$, where R is the distance from the origin, through the relation

$$\Phi^{(1)}(R = R_\infty) = -(\nabla_R \Phi)_{R=R_\infty} R_\infty. \quad (24)$$

The procedure is then repeated till a convergence criteria is satisfied; in the present case the criteria are given by a difference of the integral

$$I_1 = \int \nabla_n \Phi dS \quad (25)$$

over the drop surface, calculated in two subsequent steps, lower than 10^{-5} .

To notice that for a perfectly spherically symmetric problem, it can be easily shown that the method converges to the exact solution. For nonspherically symmetric problems, like those analyzed here, the value $\Phi_\infty^{(n)}$ to be imposed at the n th step on the outer surface is taken as a surface average of the distribution given by Eq. (24), and the procedure converges to an approximate solution. To check the accuracy of this method, numerical solutions are first compared with exact analytical solutions for the case of a single sessile drop [Eq. (12)] and of a pair of identical suspended (free) drops, which can be found, for example, in [48,49].

The size of the computational domain, i.e., the value of R_∞ , was set assuring that the boundary conditions at free stream are sufficiently accurate, compromising between the desirable grid refinement and the approximated uniform boundary conditions at free stream. Comparison with analytical solutions available for a single sessile drop and a pair of free drops shows that the choice of imposing the free stream conditions at a radial distance from the domain center is equal to 30 drop radii (i.e., $R_\infty = 30R_d$) yields an acceptable accuracy.

For the case of isolated drops, both suspended and sessile ones, with contact angle equal to 135° and 45° , exact analytical solutions of the problem are available [Eq. (12)] and used as benchmark for the numerical calculations. A grid independence analysis was performed, refining the computational mesh up to 1.54 million elements. The discrepancy between the evaporation rate predicted by the numerical calculations and by the exact analytical solution was lower than 7×10^{-5} for the single suspended drop and lower than 6×10^{-5} and 1×10^{-4} for the sessile drop with contact angle equal to 135° and 45° , respectively. An excellent agreement among the numerical predictions and the exact analytical solutions is obtained also in the more critical case of hydrophilic condition, where the vapor flux on the drop surface, which is proportional to the gradient of the function Φ , becomes infinite approaching the triple line (see, for example, [50]), as shown in Fig. 6.

To test the accuracy of the numerical solution for the case of a drop pair, the case of two suspended identical drops (formally identical to the case of a drop pair with contact angle equal to $\pi/2$) with drop separation distance $\lambda_2 = \frac{\lambda_0}{R_d}$ (refer to Fig. 1) varying from 2 to 10 was considered since an exact analytical solution of the Laplace equation is available, as mentioned above.

Table I reports the results in terms of the screening coefficient, defined as the ratio between the evaporation rate

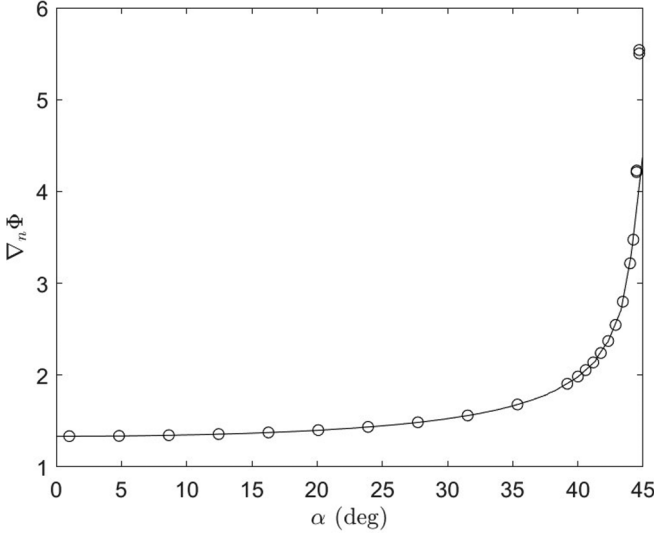


FIG. 6. Surface nondimensional flux as function of angular position, α (see Fig. 1), from numerical (line) and analytical (symbols) solutions; hydrophilic substrate with $\theta_c = 45^\circ$.

from one of the two interacting drops and the corresponding value from a single drop [49], as predicted by the analytical solution and by the numerical model. The results confirm that the accuracy of the numerical solution is better than 7×10^{-4} for all the test cases selected.

Having assessed the accuracy of the numerical solution for the cases relevant to the present investigation, the numerical solution is now taken as reference for the assessment of the analytical model proposed in the previous section.

Again two contact angles equal to 135° and 45° and three values of the separation distance λ_2 from 2 to 10 have been analyzed. The results are reported in Table I, showing a good agreement among the numerical and the analytical predictions, with an average relative difference of 2.8×10^{-3} and a maximum relative difference of the order of 7×10^{-3} . Figure 7 summarizes the previous results, reporting the three curves corresponding to the screening coefficients for the three sessile drop configurations with varying drop interdistance from 2 to 10, as predicted by the analytical solutions and the corresponding values from the numerical model, confirming the rather good agreement among the results for the range of operating conditions selected.

This comparison shows the capability of the simple analytical model, Eq. (15), to predict the effect of neighboring drops on their evaporation characteristics.

TABLE I. Screening coefficient calculated by the analytical solution, γ^a , and by the numerical model, γ^n , for three sessile drop configurations and three nondimensional distance, λ_2 .

λ_2	$\theta_c = 90^\circ$		$\theta_c = 135^\circ$		$\theta_c = 45^\circ$	
	γ^a	γ^n	γ^a	γ^n	γ^a	γ^n
2	0.8024	0.8026	0.7670	0.7728	0.8859	0.8829
5	0.9086	0.9092	0.8853	0.8873	0.9506	0.9497
10	0.9524	0.9524	0.9393	0.9395	0.9766	0.9742

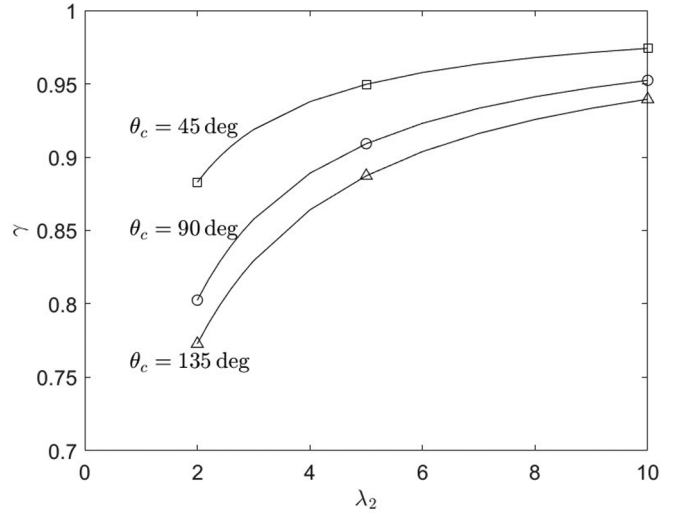


FIG. 7. Screening coefficient as function of nondimensional distance λ_2 for three drop configurations as predicted by the analytical model (line) and by the numerical calculation (symbols).

IV. COMPARISON WITH SOME EXPERIMENTAL RESULTS

The predictions of the proposed model can be compared to available experimental data, like those reported in [23], where pairs of deionized water sessile drops deposited on hydrophobic substrates (polydimethylsiloxane) were observed to evaporate in air at ambient conditions (25°C and 40%–50% relative humidity). Contact angles, θ_c , contact radii, R_c , and drop volumes, V , were measured for single drops and for three different center-to-center drop pair distances (see Table II). Measurements of the ratios $\theta_c/\theta_{c,0}$, $R_c/R_{c,0}$, and V/V_0 (where $R_{c,0}$, $\theta_{c,0}$, and V_0 are the initial contact radius, contact angle, and volume, respectively) are reported in the paper versus nondimensional time $\tau = t/t_{1d}$, where t is the time and t_{1d} is the evaporation time of the single sessile drop. The initial contact angle is 115° , but during evaporation the drops undergo different evaporation regimes; precisely the constant contact radius (CCR) regime is observed at the beginning, followed by the constant contact angle (CCA) and the mixed regimes. In the time period $\tau \in (0-0.6)$ the contact angle changes from the initial value to about 0.77 times the initial angle (i.e., $\approx 90^\circ$), and the nondimensional distance L/D (where $D = 2R_d$ is the drop equatorial diameter) changes, due to drop shrinking caused by evaporation. The value of $\lambda_2 = \frac{x_0}{R_d}$ (see Fig. 2) was reported to change [Fig. 4(d) of [23]], and an

TABLE II. Initial nondimensional distance $\lambda_{2,0}$, average time derivative of V/V_0 , linear correlation coefficient R^2 , average nondimensional distance $\bar{\lambda}_2$, screening coefficient; data from [23].

$\lambda_{2,0} = L/D$	$\frac{d(V/V_0)}{d\tau}$	R^2	$\bar{\lambda}_2$	γ
∞	1.3365	0.9586		
1.6	1.1132	0.9392	1.84	0.83
1.3	0.7702	0.993	1.40	0.58
1.2	0.7491	0.9872	1.23	0.56

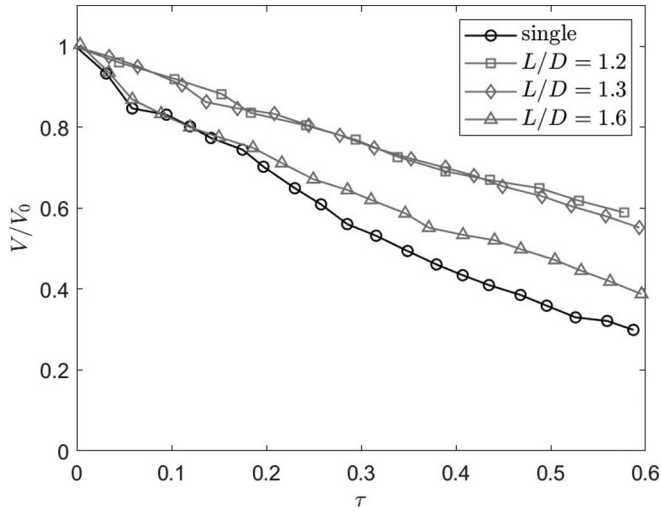


FIG. 8. Value of the ratio V/V_0 as reported in Fig. 4(a) of [23], for the nondimensional time interval $\tau \in (0 - 0.6)$.

average value over the evaporation period can be calculated from the reported data (see Table II).

The variation of V/V_0 with time for the single sessile drop case shows a nonlinear behavior; however, when the time interval $\tau \in (0, 0.6)$ is considered, linearity may be assumed as a first approximation, for the single drop and for the other cases as well, as reported in Fig. 8 [data are obtained from Fig. 4(a) of [23]].

The average values of $\frac{d(V/V_0)}{d\tau}$ over the time period $\tau \in (0, 0.6)$ can be estimated as best linear fit, and the results are reported in Table II, where the values of the linear correlation coefficient, R^2 , are also reported, and their high values (from 0.96 to 0.99) justify the procedure. Table II also reports the value of $\lambda_2 = \frac{x_0}{R_d}$ averaged over the period $\tau \in (0, 0.6)$.

Since $\frac{d(V/V_0)}{d\tau}$ is proportional to the mean evaporation rate, the ratio between the values corresponding to the three different drop pair configurations and that corresponding to the single drop case yields an estimation of the average screening coefficient γ (see Table II). Figure 9 reports the values of γ as a function of the average nondimensional distance $\bar{\lambda}_2$ and the corresponding values calculated from the proposed analytical model for both the initial and final contact angles (115° and 90° , respectively).

The discrepancies between measured and estimated values should be judged considering the simplifying assumptions of the proposed model and the variability of the measured data, in particular the reported asymmetry of the configuration during evaporation and the possible presence of free convection effects due to the low molar mass of the evaporating species with respect to air.

Two sets of experimental data on a linear array made of three evaporating sessile drops (see Fig. 4) are found in the literature, and the reported information allows a comparison with the proposed model.

In [21] measurements of $\theta_c/\theta_{c,0}$, $R_c/R_{c,0}$, and V/V_0 are reported for the central drop, as a function of the nondimensional time $\tau = t/t_{1d}$ (where again t_{1d} is the lifetime of a single sessile drop) for initial values of $\lambda_2 = \frac{L}{D} = \frac{x_0}{R_d}$

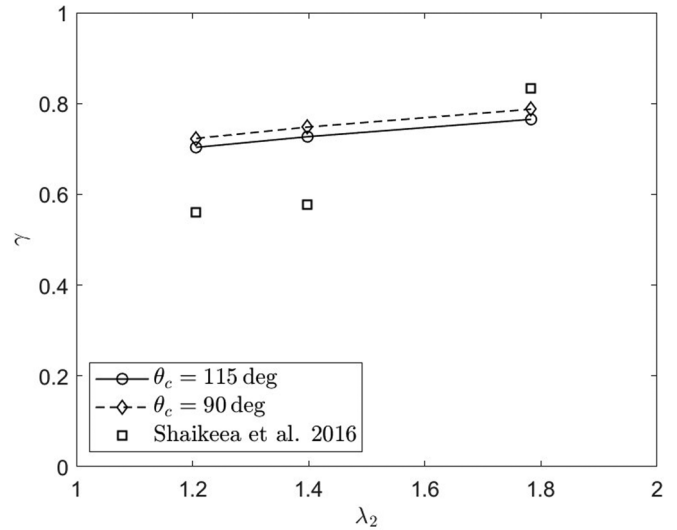


FIG. 9. Comparison between the screening factors γ as obtained from the experimental data reported in [23] and those calculated by the proposed model.

ranging from 1.1 to 2.6 and for a single sessile drop. Polydimethylsiloxane (PDMS) substrate was used, which yields an initial contact angle $\theta_c = 110^\circ \pm 2^\circ$. The initial drop volume ($V_0 = 2 \mu\text{l}$) yields an initial value of R_c (the radius of the sessile drop base; see Fig. 2) of about 0.75 mm. Also in the present case, the initial evaporation mode is CCR (as can be observed from the measurements reported in [21]), followed by some period of CCA and mixed regimes.

The drop volume variation with time $V(t)$ is reported in Fig. 10 (from [21]), and it can again be linearly fitted, over the whole evaporation period for all the cases with quite high values of the linear correlation coefficient (see Table III). Following the above mentioned procedure, an average value of $\frac{dV/V_0}{d\tau}$ can be obtained by a linear interpolation for all reported cases (see Table III).

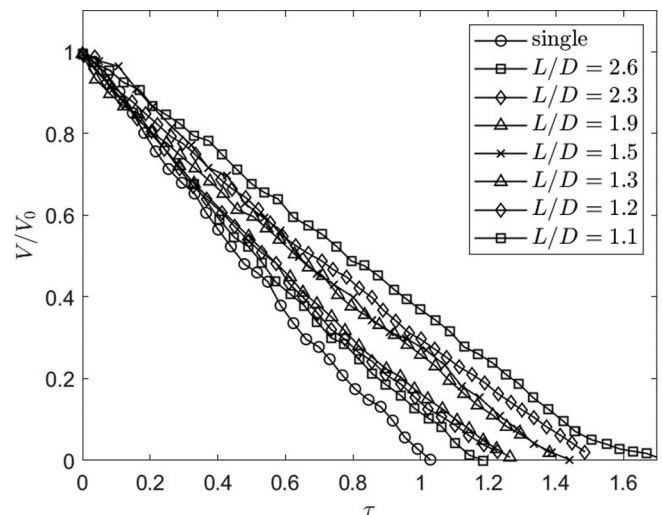


FIG. 10. Transient profiles of drop nondimensional volume for a single drop and seven values of drop interdistance configurations, from [21].

TABLE III. Initial nondimensional distance $\lambda_{2,0}$, average time derivative of V/V_0 , linear correlation coefficient R^2 , average nondimensional distance $\bar{\lambda}_2$, screening coefficient of the central drop from experiments and the numerical model setting θ_c equal to 88° and 110° ; data from [21].

$\lambda_{2,0} = L/D$	$\frac{dV/V_0}{dt}$	R^2	$\bar{\lambda}_2$	$\gamma_c(\text{exp})$	$\gamma_c(88^\circ)$	$\gamma_c(110^\circ)$
∞	1.018	0.9942	—	—	—	—
2.6	0.9055	0.9891	3.25	0.889	0.755	0.723
2.3	0.8678	0.9857	2.87	0.852	0.726	0.692
1.9	0.8448	0.9861	2.15	0.830	0.662	0.620
1.5	0.7272	0.9952	1.92	0.714	0.626	0.588
1.3	0.7486	0.989	1.63	0.735	0.582	0.539
1.2	0.6909	0.9923	1.46	0.679	0.546	0.505
1.1	0.6237	0.9972	1.30	0.613	0.514	0.472

The initial angle is reported to be 110° , while the final one is about 0.8 times (i.e., 88°), as can be deduced by the data reported in Fig. 3(b) of [21]. Also the values of λ_2 are not constant, since they increase with time due to drop

shrinking. Direct measurements of λ_2 during the evaporation are not available, but considering that the ratios $\hat{\theta} = \theta_c/\theta_{c,0}$ and $\hat{R} = R_c/R_{c,0}$ are reported and

$$\lambda_2(t) = \frac{L}{D(t)} = \frac{L}{D_0 \frac{R_d}{R_{d,0}}} = \lambda_{2,0} \frac{\sin \theta}{\frac{R_c \sin \theta_0}{R_{c,0}}} = \lambda_{2,0} \frac{\sin(\hat{\theta} \theta_0)}{\hat{R} \sin \theta_0} \quad (26)$$

a time average value of λ_2 can be calculated, for each drop configuration, from the measurements and the values are listed in Table III.

The screen factors γ_c obtained from the experiments can be compared to those calculated from the model, for the range of contact angles between the initial (110°) and the final (88°), as shown in Table III.

Measurements on evaporating drop arrays with different configurations are reported in [24], for a contact angle equal to 90° (maintained constant by electrowetting methods), and the cases of single drop and three drops configuration are considered, together with more complex configurations. The measurement results are given in their Fig. 4 in terms of the square of the contact radius as a function of time, and

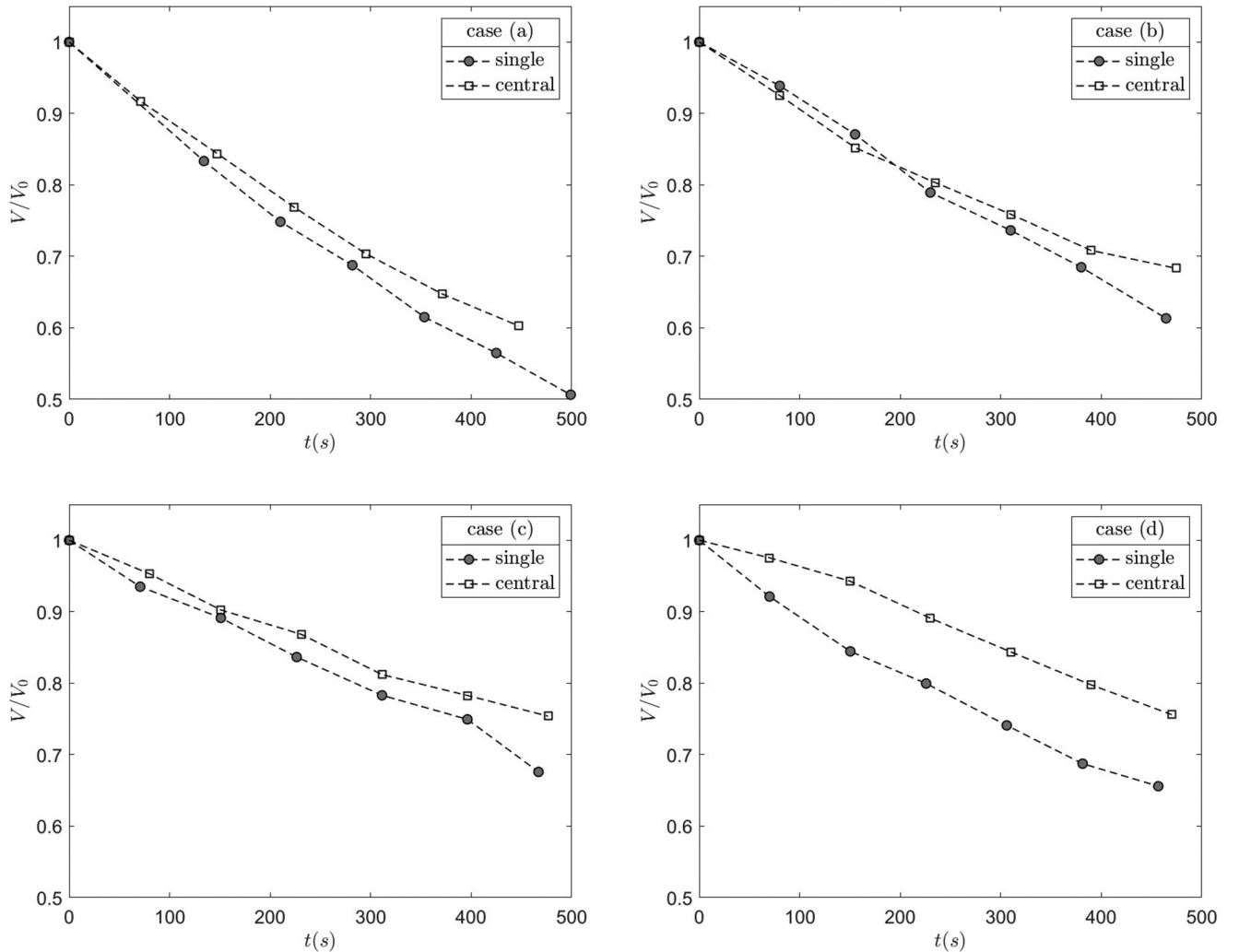


FIG. 11. Experimental values of $V/V_0 = (R_d/R_{d,0})^3$ versus time, as obtained from the data reported in Fig. 4 of [24], for a single drop (solid circle) and for the central drop of a triplet (open squares), for four different confinements (see [24] for details).

TABLE IV. Initial nondimensional distance $\lambda_{2,0}$, average time derivative of V/V_0 , linear correlation coefficient R^2 , average nondimensional distance $\bar{\lambda}_2$, screening coefficient of the central drop from experiments and the numerical model; data from [24].

Case	$\lambda_{2,0}$	$\frac{dV/V_0}{dt}$ (s^{-1})	R^2	$\bar{\lambda}_2$	$\gamma_c(\text{exp})$	$\gamma_c(\text{mod.})$
a	∞	$1.1056 \cdot 10^{-3}$	0.982	—	—	—
	4.75	$0.9457 \cdot 10^{-3}$	0.977	5.161	0.867	0.831
b	∞	$0.855 \cdot 10^{-3}$	0.997	—	—	—
	4.75	$0.7455 \cdot 10^{-3}$	0.951	5.046	0.831	0.827
c	∞	$0.6779 \cdot 10^{-3}$	0.977	—	—	—
	4.75	$0.5511 \cdot 10^{-3}$	0.980	4.959	0.804	0.825
d	∞	$0.8183 \cdot 10^{-3}$	0.966	—	—	—
	4.75	$0.5088 \cdot 10^{-3}$	0.991	4.997	0.650	0.826

they are reproduced in Fig. 11, in terms of $V/V_0 = (R_c/R_{c,0})^3$ (since in this case $R_c = R_d$) as a function of time.

The four cases refer to different drop confinements, obtained by positioning a lid over the drops at various distances (see [24] for the details). The time profiles for some of the cases show an evident nonlinearity; however, limiting the analysis at the time interval 0–500 s the data can be linearly fitted to evaluate the average time derivative of V/V_0 , which is proportional to the average evaporation rate, with good values of the linear correlation coefficient R^2 , which spans from 0.966 to 0.997, justifying the approach. The results are reported in Table IV.

The initial value of λ_2 was 4.75, but the drop shrinking causes an increase of λ_2 since

$$\lambda_2 = \frac{L}{D} = \frac{L}{D_0 \frac{R_d(t)}{R_{d,0}}} = \frac{\lambda_{2,0}}{\frac{R_d(t)}{R_{d,0}}} \quad (27)$$

that can be calculated from the data available in [24], and the average value over the interval $t \in (0-500)$ s is also reported in Table IV for the four cases. Table IV also shows the experimental values of the screening coefficient γ_c (central drop), calculated again as the ratio between the values of $\frac{dV/V_0}{dt}$ for the central drop and the single drop case obtained from the experiments, as well as the values calculated from the analytical model. It can be observed that for the last case (d) the experimental value of the screening coefficient is much lower than the others and it is worth mention that this case corresponds to the presence of an horizontal lid positioned at 3 mm over the drop, which may alter the evaporation characteristics (see [24] for details of the experiments).

The values of the screening coefficients for the three-drop configuration, calculated from the measurements reported in [21] and [24], are shown in Fig. 12, together with the predictions from the model.

Again, the discrepancies should be judged taking into account the simplifying hypotheses of the analytical model and the inherent variability of the measured data.

V. EXTENSION TO ARRAYS OF IDENTICAL SESSILE DROPS

The model above proposed can be extended to an arbitrary number of sessile drops, and this section reports a guideline

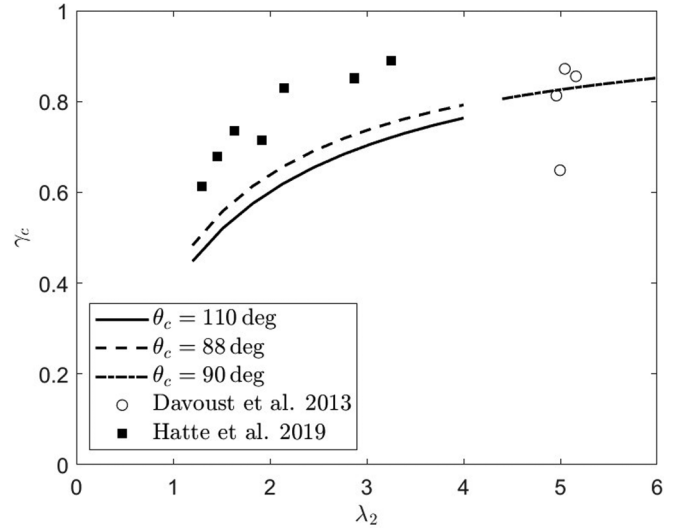


FIG. 12. Values of the screening coefficient γ_c for the central drop of a triplet of sessile drops, as obtained from the data reported in [21] (solid circles) and [24] (open squares) and calculated through the analytical approach (lines).

to such an extension, considering N identical sessile drops over a substrate. Let us assume than the coordinates of the k th sessile drop center (intended as the center of the circular contact surface) are given by (x_k, y_k) . The exact solution to the Laplace equation for a single drop positioned at (x_k, y_k) is

$$\Phi_k(x, y, z) = \Phi(x - x_k, y - y_k, z), \quad (28)$$

where $\Phi(x, y, z)$ is the solution for the same drop centered at the origin. The superposition

$$\Phi_T(x, y, z) = \sum_k \gamma_k \Phi_k(x, y, z) \quad (29)$$

is still a solution of the Laplace equation, which is nil at infinity. It is possible to choose γ_j such that the boundary condition on the liquid surface ($\Phi = 1$) is satisfied at least on some points of the drop surfaces. Following the method previously adopted for the drop pairs and triplets, the values of γ_j can be found assuming that the boundary condition $\Phi_T = 1$ is satisfied on all drop apices, yielding the system of N equations:

$$1 = \sum_k \gamma_k \Phi_k(x_p - x_k, y_p - y_k, z_0 + R_d). \quad (30)$$

Defining

$$\Phi_{pk} = \Phi_k(x_p - x_k, y_p - y_k, z_0 + R_d), \quad (31)$$

the linear system can be written as

$$\sum_k \Phi_{pk} \gamma_k = 1, \quad (32)$$

and an inversion of the matrix Φ_{pk} yields the values of all γ_k and then the solution.

To notice that $\Phi_{pk} = \Phi_{kp}$, and since $\Phi_k(0, 0, z_0 + R_d) = 1$, then the values on the diagonal are all unitary, thus only $\frac{(N-1)N}{2}$ values of the function Φ must be calculated.

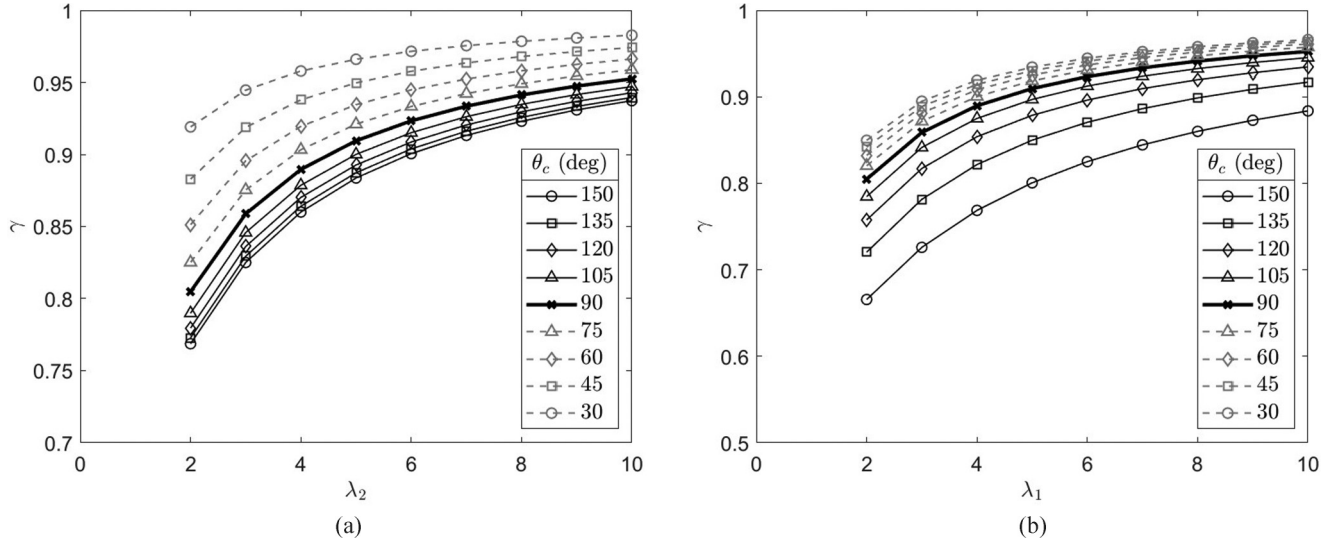


FIG. 13. Screening factor γ predicted by the analytical model as a function of (a) $\lambda_2 = x_0/R_d$ and (b) $\lambda_1 = x_0/R_c$, for different values of the contact angle.

The model can also be extended to nonidentical drops following a similar path; however, analysis and validation of the model for drop arrays are beyond the scope of the present paper and will not be discussed here.

VI. RESULTS AND DISCUSSION

In the previous sections it has been shown that the evaporation of two adjacent drops interferes in such a way that one drop screens the other and the evaporation rate is then reduced with respect to a single drop under the same conditions. The screening coefficient, γ , defined as the ratio of the evaporation rate of one of the two drops and that of the single evaporating drops, is shown to be, at least in the absence of external convection but under the effect of the Stefan flow, a geometric quantity, since the effects of the thermophysical properties are wiped out. Also the dependence on the drop size is canceled out by the linear dependence of the evaporation rate on the drop radius, and then the remaining quantities can be grouped into two nondimensional parameters that define the screening coefficient of a pair of identical sessile drops: the contact angle, θ_c , and the nondimensional drop separation. This last parameter can be defined in at least two different ways, i.e., as the ratio of the distance between the two drop centers and the contact radius, R_c , or the curvature radius, R_d . To maintain a connection with the same quantity defined for free drops (see, for example, [48,49,51]) the following two definitions are considered:

$$\lambda_1 = \frac{L}{2R_c}, \quad (33a)$$

$$\lambda_2 = \frac{L}{2R_d}, \quad (33b)$$

which are related to each others by (see Fig. 1)

$$\lambda_1 = \frac{L}{2R_c} = \frac{L}{2R_d \sin(\psi_0)} = \frac{\lambda_2}{\sin(\theta_c)}. \quad (34)$$

From a geometric point of view the two definitions are equivalent; clearly for drops on hydrophobic substrates λ_2 has an evident lower boundary independent of the contact angle and equal to one (which is not true for λ_1 in this case), whereas for the case of sessile drops on hydrophilic substrates it is λ_1 that has a lower boundary independent of the contact angle, and again equal to one. In any case the screening coefficient, under the assumptions made in the present analysis, is a function of θ_c and λ_1 or λ_2 .

Using Eq. (15), which, as above described, has been numerically assessed and tested against experimental values, the screening factor γ was evaluated for different values of the contact angle and different nondimensional separations λ_1 and λ_2 , and the results are reported in Fig. 13.

It can be observed that for sessile drops on hydrophilic substrates the parameter λ_1 groups the resulting curve better than λ_2 and vice versa for hydrophobic substrates.

Drops on hydrophobic substrates show a larger screening effect than drops on hydrophilic ones, which could possibly be connected to the larger protrusion of these drops in the vapor field when compared to drops with lower contact angle. However, a more consistent comparison should be done between drops with the same volume deposited on different substrates. To this end, consider a drop with a given volume V ; under the assumption of negligible effect of gravity the following relations hold:

$$V = \pi R_c^3 \frac{2 - 3 \cos(\theta_c) + \cos^3(\theta_c)}{3 \sin^3(\theta_c)}, \quad (35)$$

$$R_{eq} = \left(\frac{3V}{4\pi} \right)^{1/3} = R_c \left(\frac{2 - 3 \cos(\theta_c) + \cos^3(\theta_c)}{4 \sin^3(\theta_c)} \right)^{1/3}, \quad (36)$$

where R_{eq} is the radius of a spherical drop having the same volume of the sessile one.

Given two drops of a given volume V at a distance L from each other, it is then possible to analyze the effect of

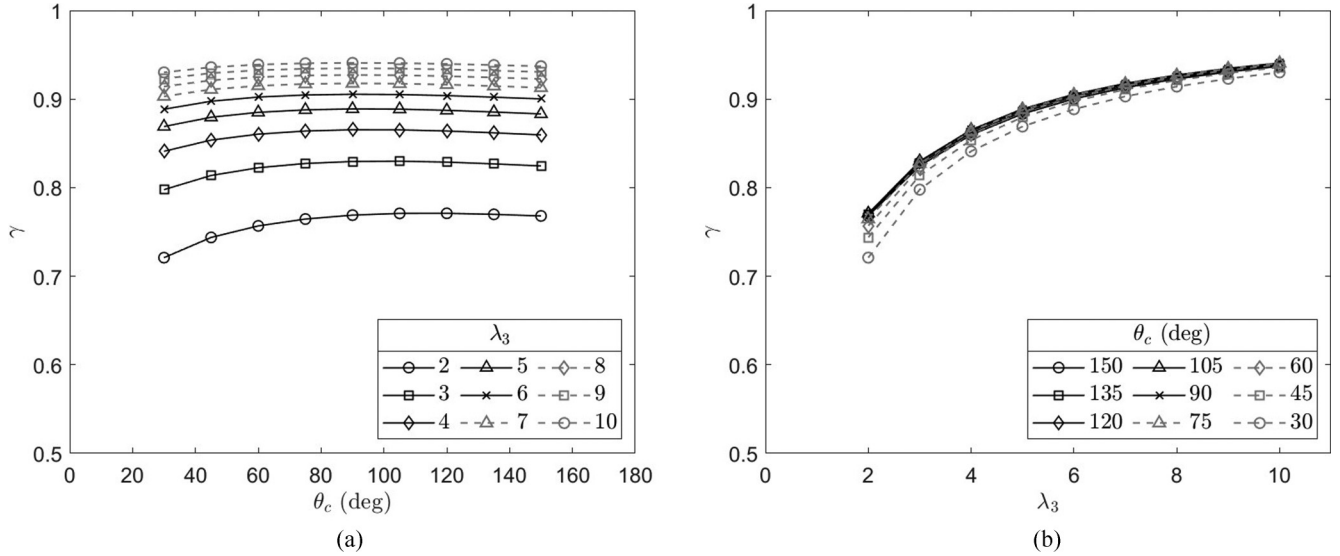


FIG. 14. (a) Values of the screening factor γ as a function of the contact angle, for different values of $\lambda_3 = x_0/R_{eq}$. (b) Values of the screening factor γ as a function of the nondimensional drop distance $\lambda_3 = x_0/R_{eq}$, for different values of the contact angle.

wettability on screening. Defining $\lambda_3 = \frac{L}{2R_{eq}}$ the screening coefficient can be calculated for any value of λ_3 as a function of wettability. To notice that for each value of λ_3 there exists an angle $\theta_{c,min}$ under which the sessile drops interfere.

Figure 14(a) reports the values of screening coefficient γ as a function of the contact angle for different values of λ_3 , showing that for a given volume and distance, the screening factor is lower for drops on hydrophilic substrate, i.e., the opposite of what could be simplistically inferred from Fig. 13.

The effect becomes larger for smaller values of λ_3 , i.e., smaller drop interdistances.

The effect of wettability on the screening can be interpreted observing that for any given drop volume, the outer edges of drops are closer for drops on hydrophilic substrates; moreover the evaporation fluxes diverge on the triple line [50], and this causes a stronger interaction between the evaporation fluxes.

It can also be noticed from Fig. 14(b) that the curves collapse together when using λ_3 as the nondimensional measure of the drop interdistance, particularly for hydrophobic drops: the difference between the screening factors at $\theta_c = 150^\circ$ and $\theta_c = 90^\circ$ is less than 0.6% for $\lambda_3 \geq 2$. This finding may suggest the use of $\lambda_3 = \frac{L}{2R_{eq}}$, rather than other nondimensional distances, to better compare the effect of distance on drop evaporation screening for different substrate wettability.

As a final analysis, a comparison with the asymptotic solution proposed for thin drops in [32] can be done. In the theoretical work of [32], the evaporation of arrays of thin drops of circular shape were considered, and explicit analytical expressions for the local and integral vapor fluxes were given. This kind of shape is found where the drop size is larger than the capillary length so that the drop spread under the effect of gravity forms a thin film. The solution for case of a pair of identical drops was reported and an explicit expression for the screening coefficient of the drop pair can be deduced from their Eq. (3.4), and it can be written as

$$\gamma = \frac{1}{1 + \frac{2}{\pi} \arcsin\left(\frac{1}{2\lambda_1}\right)}. \quad (37)$$

It should be noticed that in [32] the mass transfer is modeled as purely diffusive and the Stefan flow is neglected; however, the ratio between the evaporation rate from one of the twin drops and that of an isolated drop, which is the screening coefficient, yields a correct value since the Stefan flow is neglected in both cases. The resulting values of the screening coefficient for different drop interdistance are compared in Fig. 15 with that obtained by the present modeling, for drops on hydrophilic substrate with vanishing contact angle (from 30° to 10°). It can be clearly observed that the results of [32] represent an asymptote, for $\theta_c \rightarrow 0$, for the values predicted by the present modeling.

It is then of a certain interest to note that the present approach, in connection with the cited modeling of thin drops evaporation [32], may allow to extend the range of application

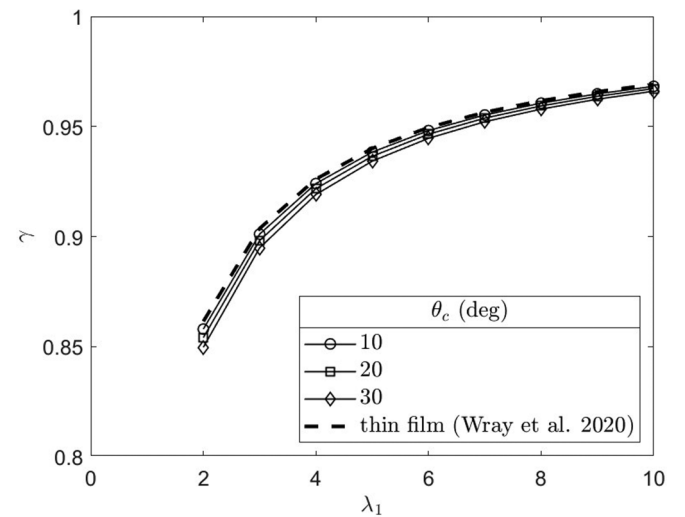


FIG. 15. Values of the screening factor γ as a function of the nondimensional drop distance $\lambda_1 = x_0/R_c$, for three values of the contact angle (30° , 20° , 10°) and the thin film prediction from [32].

of multiple drop evaporation analytical modeling, from very low to very high contact angle conditions.

VII. CONCLUSIONS

The paper reports a simple analytical approach to model the evaporation of pairs and triplets of sessile drops. The solution to the gas phase species and energy conservation equations in toroidal coordinates is extended to the case of two and three identical sessile drops.

The evaporation rates from each sessile drop in the array are compared to those for single drops with the same contact angle to yield a screening coefficient that quantifies the evaporation reduction due to drop vicinity. The analytical solution is assessed by comparison with accurate numerical solutions. The discrepancy between the analytical values of the screening coefficients and the numerical ones is comparable to the accuracy of the numerical solutions for interdistance larger than about 5 times the base drop radius for drops on hydrophobic substrates, while for closer drops the maximum discrepancy is of the order of 7×10^{-3} . The cases of drops on hydrophilic substrates present a criticality due to the flux that becomes infinite at the triple line, although the discrepancy among the analytical values of the screening coefficients and

the numerical ones is always lower than 3.5×10^{-3} for all the selected operating conditions.

The model is validated against three sets of experimental data, for two and three evaporating drops on a line. The average screening coefficient obtained from the available experimental data is compared to that predicted by the model and the comparison appears satisfactory, despite the simplifying assumptions of the model and the reported experimental uncertainties.

The model is then used to quantify the shielding effect on drop evaporation for pairs of sessile droplets as a function of drop interdistance and contact angle, in a relatively wide range of values. It was observed that for hydrophobic substrates the decrease of evaporation rate is larger than 5% even when the drop interdistance is equal to 10 drop equatorial diameters. For hydrophilic substrates a comparable effect is found when the drop interdistance is equal to 10 times the diameter of the drop base. The use of a nondimensional drop separation parameter, defined as the ratio between the drop interdistance and the equivalent volume diameter, $\lambda_3 = \frac{L}{2R_{eq}}$, allows us to quantify the effect of drop neighboring on drop pair evaporation in a way that is almost independent of wall wettability.

A way to extend the proposed analytical model to the case of an arbitrary number of drops is reported.

-
- [1] J. Park and J. Moon, Control of colloidal particle deposit patterns within picoliter droplets ejected by ink-jet printing, *Langmuir* **22**, 3506 (2006).
- [2] Y. Yu, H. Zhu, J. M. Frantz, M. E. Reding, K. C. Chan, and H. E. Ozkan, Evaporation and coverage area of pesticide droplets on hairy and waxy leaves, *Biosyst. Eng.* **104**, 324 (2009).
- [3] D. Xia and S. R. J. Brueck, Strongly anisotropic wetting on one-dimensional nanopatterned surfaces, *Nano Lett.* **8**, 2819 (2008).
- [4] E. Y. Gatapova, A. M. Shonina, A. I. Safonov, V. S. Sulyaeva, and O. A. Kabov, Evaporation dynamics of a sessile droplet on glass surfaces with fluoropolymer coatings: Focusing on the final stage of thin droplet evaporation, *Soft Matter* **14**, 1811 (2018).
- [5] Z. Chen, Q. Xie, G. Chen, Y. Yu, and Z. Zhao, Numerical simulation of single-nozzle large scale spray cooling on drum wall, *Thermal Sci.* **22**, 359 (2018).
- [6] M. Chopra, L. Li, H. Hu, M. A. Burns, and R. G. Larson, DNA molecular configurations in an evaporating droplet near a glass surface, *J. Rheol.* **47**, 1111 (2003).
- [7] H. Y. Erbil, Evaporation of pure liquid sessile and spherical suspended drops: A review, *Adv. Colloid Interface Sci.* **170**, 67 (2012).
- [8] D. Brutin and V. Starov, Recent advances in droplet wetting and evaporation, *Chem. Soc. Rev.* **47**, 558 (2018).
- [9] P. Gurrula, S. Balusamy, S. Banerjee, and K. C. Sahu, A review on the evaporation dynamics of sessile drops of binary mixtures: Challenges and opportunities, *Fluid Dyn. Materials Proc.* **17**, 253 (2021).
- [10] R. T. van Gaalen, C. Diddens, H. M. A. Wijshoff, and J. G. M. Kuerten, Marangoni circulation in evaporating droplets in the presence of soluble surfactants, *J. Colloid Interface Sci.* **584**, 622 (2021).
- [11] N. Murisic and L. Kondic, On evaporation of sessile drops with moving contact lines, *J. Fluid Mech.* **679**, 219 (2011).
- [12] T. W. G. van der Heijden, A. A. Darhuber, and P. Van Der Schoot, Macroscopic model for sessile droplet evaporation on a flat surface, *Langmuir* **34**, 12471 (2018).
- [13] G. J. Dunn, S. K. Wilson, B. R. Duffy, S. David, and K. Sefiane, The strong influence of substrate conductivity on droplet evaporation, *J. Fluid Mech.* **623**, 329 (2009).
- [14] R. D. Deegan, O. Bakajin, T. F. Dupont, G. Huber, S. R. Nagel, and T. A. Witten, Contact line deposits in an evaporating drop, *Phys. Rev. E* **62**, 756 (2000).
- [15] R. G. Picknett and R. Bexon, The evaporation of sessile or pendant drops in still air, *J. Colloid Interface Sci.* **61**, 336 (1977).
- [16] M. E. Shanahan, Simple theory of “stick-slip” wetting hysteresis, *Langmuir* **11**, 1041 (1995).
- [17] E. Bormashenko, A. Musin, and M. Zinigrad, Evaporation of droplets on strongly and weakly pinning surfaces and dynamics of the triple line, *Colloids Surf. A* **385**, 235 (2011).
- [18] Y. S. Yu, Z. Wang, and Y. P. Zhao, Experimental and theoretical investigations of evaporation of sessile water droplet on hydrophobic surfaces, *J. Colloid Interface Sci.* **365**, 254 (2012).
- [19] J. M. Stauber, S. K. Wilson, B. R. Duffy, and K. Sefiane, On the lifetimes of evaporating droplets, *J. Fluid Mech.* **744**, R2 (2014).
- [20] N. N. Lebedev, *Special Functions & Their Applications* (Dover, New York, 1972).
- [21] S. Hatte, K. Pandey, K. Pandey, S. Chakraborty, and S. Basu, Universal evaporation dynamics of ordered arrays of sessile droplets, *J. Fluid Mech.* **866**, 61 (2019).

- [22] D. Khilifi Sadok, W. Foudhil, K. Fahem, S. Harmand, and J. S. Ben, Study of the phenomenon of the interaction between sessile drops during evaporation, *Thermal Sci.* **23**, 1105 (2019).
- [23] A. J. D. Shaikeea and S. Basu, Insight into the evaporation dynamics of a pair of sessile droplets on a hydrophobic substrate, *Langmuir* **32**, 1309 (2016).
- [24] L. Davoust and J. Theisen, Evaporation rate of drop arrays within a digital microfluidic system, *Sensors Actuators B: Chemical* **189**, 157 (2013).
- [25] M. Sokuler, G. K. Auernhammer, C. J. Liu, E. Bonaccorso, and H.-J. Butt, Dynamics of condensation and evaporation: effect of inter-drop spacing, *Europhys. Lett.* **89**, 36004 (2010).
- [26] C. Schäffle, C. Bechinger, B. Rinn, C. David, and P. Leiderer, Cooperative Evaporation in Ordered Arrays of Volatile Droplets, *Phys. Rev. Lett.* **83**, 5302 (1999).
- [27] O. Carrier, N. Shahidzadeh-Bonn, R. Zargar, M. Aytouna, M. Habibi, J. Eggers, and D. Bonn, Evaporation of water: Evaporation rate and collective effects, *J. Fluid Mech.* **798**, 774 (2016).
- [28] A. M. Lacasta, I. M. Sokolov, J. M. Sancho, and F. Sagués, Competitive evaporation in arrays of droplets, *Phys. Rev. E* **57**, 6198 (1998).
- [29] V. I. Fabrikant, On the potential flow through membranes, *Z. Angew. Math. Phys.* **36**, 616 (1985).
- [30] I. I. Argatov, Electrical contact resistance, thermal contact conductance and elastic incremental stiffness for a cluster of microcontacts: Asymptotic modelling, *Q. J. Mech. Appl. Math.* **64**, 1 (2011).
- [31] B. Dollet and D. Lohse, Pinning stabilizes neighboring surface nanobubbles against Ostwald ripening, *Langmuir* **32**, 11335 (2016).
- [32] A. W. Wray, B. R. Duffy, and S. K. Wilson, Competitive evaporation of multiple sessile droplets, *J. Fluid Mech.* **898**, A1 (2020).
- [33] A. M. Edwards, J. Cater, J. J. Kilbride, P. Le Minter, C. V. Brown, D. J. Fairhurst, and F. F. Ouali, Interferometric measurement of co-operative evaporation in 2D droplet arrays, *Appl. Phys. Lett.* **119**, 151601 (2021).
- [34] G. E. Cossali and S. Tonini, An analytical model of heat and mass transfer from liquid drops with temperature dependence of gas thermo-physical properties, *Int. J. Heat Mass Transf.* **138**, 1166 (2019).
- [35] J. C. Slattery, *Momentum, Energy and Mass Transfer in Continua* (R. Krieger, New York, 1981).
- [36] R. Bird, W. Stewart, and E. Lightfoot, *Transport Phenomena* (John Wiley and Sons, New York, 2002).
- [37] S. Tonini and G. E. Cossali, Analytical solutions for modelling the evaporation of sessile drops (unpublished).
- [38] F. W. J. Olver, D. W. Lozier, R. F. Boisvert, and C. W. Clark (eds.), *NIST Handbook of Mathematical Functions* (Cambridge University Press, Cambridge, 2010).
- [39] Y. Popov, Evaporative deposition patterns: Spatial dimensions of the deposit, *Phys. Rev. E* **71**, 036313 (2005).
- [40] S. F. Chini and A. Amirfazli, Resolving an ostensible inconsistency in calculating the evaporation rate of sessile drops, *Adv. Colloid Interface Sci.* **243**, 121 (2017).
- [41] G. E. Cossali and S. Tonini, Analytical modelling of drop heating and evaporation in drop clouds: Effect of temperature dependent gas properties and cloud shape, *Int. J. Heat Mass Transf.* **162**, 120315 (2020).
- [42] L. N. Teixeira, G. E. Crippa, R. Gimenes, M. A. Zaghete, P. T. De Oliveira, A. L. Rosa, and M. M. Beloti, Response of human alveolar bone-derived cells to a novel poly (vinylidene fluoride-trifluoroethylene)/barium titanate membrane, *J. Mater. Sci.: Mater. Med.* **22**, 151 (2011).
- [43] S. Lee, J. S. Park, and T. R. Lee, The wettability of fluoropolymer surfaces: Influence of surface dipoles, *Langmuir* **24**, 4817 (2008).
- [44] V. Pachchigar, M. Ranjan, and S. Mukherjee, Role of hierarchical protrusions in water repellent superhydrophobic PTFE surface produced by low energy ion beam irradiation, *Sci. Rep.* **9**, 8675 (2019).
- [45] J. L. Zhang, J. A. Li, and Y. C. Han, Superhydrophobic PTFE surfaces by extension, *Macromol. Rapid Commun.* **25**, 1105 (2004).
- [46] A. Liemert, Explicit solution for the electrostatic potential of the conducting double sphere, *J. Appl. Phys.* **115**, 164907 (2014).
- [47] G. P. Tong, Electrostatics of two conducting spheres intersecting at angles, *Eur. J. Phys.* **17**, 244 (1996).
- [48] A. Umemura, S. Ogawa, and N. Oshima, Analysis of the interaction between two burning droplets, *Combust. Flame* **41**, 45 (1981).
- [49] G. E. Cossali and S. Tonini, Variable gas density effects on transport from interacting evaporating spherical drops, *Int. J. Heat Mass Transf.* **127**, 485 (2018).
- [50] H. Hu and R. G. Larson, Evaporation of a sessile droplet on a substrate, *J. Phys. Chem. B* **106**, 1334 (2002).
- [51] G. Castanet, L. Perrin, O. Caballina, and F. Lemoine, Evaporation of closely spaced interacting droplets arranged in a single row, *Int. J. Heat Mass Transf.* **93**, 788 (2016).